scientific reports

OPEN

Synergetic effect of the surface ligand and SiO$_2$ driven photoluminescence stabilization of the CH$_3$NH$_3$PbBr$_3$ perovskite magic-sized clusters

Fitri Aulia Permatasari [1], Hilma Eka Masitoh[1], Ea Cahya Septia Mahen [1,2], Bebeh Wahid Nuryadin [3], Akfiny Hasdi Aimon [1], Yana Maolana Syah [4] & Ferry Iskandar [1,5✉]

Zero-dimensional Perovskite Magic-size Clusters play crucial roles in understanding and controlling nucleation and growth of semiconductor nanoparticles. However, their metastability behavior is a critical hindrance for reliable characterizations. Here, we report the first demonstration of using an excess amount of surface ligand and SiO$_2$ as novel passivation for synthesizing the magic-sized clusters (MSCs) by the Ligand-assisted reprecipitation method. A synergetic effect between an excessed surface ligand and SiO$_2$ inhibits the protonation and deprotonation reaction between amine-based and acid-based ligand, leading to enhanced PL stability. The obtained CH$_3$NH$_3$PbBr$_3$ PMSCs/SiO$_2$ retain 70% of its initial emission intensity in ambient conditions for 20 days. This passivation approach opens an entirely new avenue for the reliable characterizations of CH$_3$NH$_3$PbBr$_3$ PMSCs, which will significantly broaden their application for understanding and controlling nucleation and growth of semiconductor nanoparticles.

The finding of so-called Magic-size clusters (MSCs) is now one of the most intriguing nanoparticles research outcomes. An accelerated development could be achieved by fully understanding the MSCs, owing to their attributed roles as intermediates in nanoparticles' formation. MSCs usually be associated with the ultrasmall nanoparticle with narrow distribution sized and a strong quantum confinement effect[1]. Compared with the conventional nanoparticles, *e.g.*, Quantum Dots (QDs), MSCs possessed unique properties such as smaller size than QDs with narrow distribution, narrow photoluminescence (PL) and narrow absorption peaks owing to their molecule-like behaviour[2–4]. MSCs perform the optical properties that notably red-shift in discrete steps as the reaction progresses before the particle growth turns into the conventional QDs. These properties have corresponded to their structure that assumes be a closed shell configuration with well-defined stoichiometry, shape, and size, as well as to occupy deep, local minima in the potential landscape.

An elusive structure and growth mechanism of the PQDs originated from MSCs has become a major obstacle for further developing the PQDs[5–7]. Thus, Perovskite MSCs (PMSCs) serve as an appropriate model system for elucidating the PQDs formation mechanism, as well as their metastability and surface-related issue[8]. However, their metastability structure hinder the elucidation process that mainly relies on the reliable characterization of MSCs. The metastability behaviour of PMSCs owing to the abundant charging defects in perovskite surface, including positive-charge defect (i.e., halide ion vacancy) and negative-charge defects (i.e., cation vacancy and PbX$_4^{2-}$ anti-site defects)[8]. The surface passivation MSCs by various capping ligands, including organic acid and amines have been reported[9,10]. It was demonstrated that the PMSCs and PQD structure could be tunning by

[1]Department of Physics, Faculty of Mathematics and Natural Sciences, Institut Teknologi Bandung, Jalan Ganesha 10, Bandung, West Java 40132, Indonesia. [2]Department of Physics Education, Faculty of Tarbiyah and Education, UIN Sunan Gunung Djati Bandung, Jl. A. H. Nasution 105, Bandung 40614, Indonesia. [3]Department of Physics, Faculty of Science and Technology, UIN Sunan Gunung Djati Bandung, Jl. A. H. Nasution 105, Bandung 40614, Indonesia. [4]Department of Chemistry, Faculty of Mathematics and Natural Sciences, Institut Teknologi Bandung, Jalan Ganesha 10, Bandung 40132, Indonesia. [5]Research Center for Nanoscience and Nanotechnology, Institut Teknologi Bandung, Jalan Ganesha 10, Bandung 40132, Indonesia. ✉email: ferry@fi.itb.ac.id

adjusting the ligand concentration ratio between acid and amines-based ligands implying the crucial role of the ligands to the MSCs formation[9,10]. Unfortunately, the dynamic nature of the interaction between PMSCs surface and capping ligands permits the ligand detachment from the PMSCs surface under various conditions[11]. A sample preparation[9], including vacuum conditioning[10,12], drying process[13], or even simple purification steps that alter the samples' ligand concentrations[14], may disrupt the initial PMCS structure concerning the reliability characterization. The ligand's highly dynamic binding state that strongly correlated to their concentration might result in various complex problems in those sample preparation. However, the conclusive mechanism of this interaction is a long, hard struggle to be solved owing to their complex interactions and a serious complication in characterization. Furthermore, it remains unclear whether the surface ligands are passivating the existing trap states or developing new ones inducing a severely PL quenching. Therefore, another strategic approach for synthesized the PMSCs with good long-term stability for reliable characterization should be considered.

Silica (SiO_2) is a versatile material usually treated as a prospective candidate to resolve the long-standing bottleneck stability issue in nanostructure materials[11,15,16]. We note that the silica encapsulation has been well documented over the last decade using in-situ and ex-situ synthetic routes to enhancing the stability of the PQDs[17–21]. However, all these methods still suffer their drawbacks that hinder the practical applications of PQDs. For example, the traditional silica coating process produced only thick shells that gather a large volume of QDs, incurring difficulties in coupling them with conventional optoelectronic platforms. Various integration processes of SiO_2 into PQDs structure generate weak interaction between SiO_2 and PQDs surfaces preserve a new surface state, reducing PL emission[22–24]. In contrast, Nakamura et al. reported that the Si capping layer on the QDs structure could serve a radiative defect state that is a plausible mechanism for enhancing the QDs' PL intensity[25]. Role of the Si to the PL properties of QDs was strongly attributed to the QD structure, including geometry and strain stress[25]. Therefore, it still highly desirable to endow SiO_2 incorporated perovskite nanostructure especially in Magic-sized cluster phase with long-term stability and elucidate their interaction. To the best of our knowledge, there has been no study reported on the SiO_2 interaction with PMSCs with enhanced PL stability.

Herein, taking advantage of an excessive amount of organic and amine-based ligands synergetic with the SiO_2 incorporation on the PMSCs surface, we developed a facile approach to produce the $CH_3NH_3PbBr_3$ PMSCs with good stability. We evaluated the effect of the SiO_2 incorporation on the optical properties of the PMSCs. Intriguingly, a synergetic effect of surface ligand and SiO_2 incorporation on PMSCs enhanced the PL stability under ambient temperature for 20 days without any significant change in size and optical properties of PMSCs. This study suggests that the obtained $CH_3NH_3PbBr_3$ PMSCs/SiO_2 with good stability is preferable as a good model, representing actual morphological and structural PMSCs to study both of PMSCs and PQDs structural and formation mechanism through a reliable characterization.

Results

Optical properties of $CH_3NH_3PbBr_3$ PMSCs and $CH_3NH_3PbBr_3$ PMSCs/SiO_2.

The perovskite samples were prepared using a ligand assisted reprecipitation (LARP) method as described in previous reports[10,26]. Excessive surface ligands comprising oleylamine and oleic acid are used as capping ligands to produce the ultrasmall size of interest[9,10]. The PL emission of the samples precipitated in room temperature exhibits a blue shift emission from 550 nm up to 450 nm in varying the ligand concentration ratio (Fig. S1). A higher concentration of Oleylamine ligand in a fixed concentration of Oleic acid, inducing a blue shift emission (Fig. S2) that was also observed and investigated comprehensively in other report[10]. It was probably due to the smaller size of the perovskite that strongly corresponds to the coordination these two ligands[10]. However, the PL intensity of the samples was decreased as increasing the Oleylamine concentration (Fig. S3). However, that a high ligand concentration could hinder the practical application owing to the long-term problem during drying process. Then, the 1:0.1 ligand concentration was selected to be further investigation owing to its high PL intensity.

In varying the precipitation temperature, the solution colour turned into a bright yellow and subsequently exhibited a luminous blue to green under 365 nm UV lamp irradiation, as shown in Fig. 1a.Their photoluminescence (PL) spectra that are shown in Fig. 1b presented that all samples exhibited a single narrow emission peak centred at 480–530 nm wavelength (blue-green light). A narrow emission peak was redshifted in increasing the precipitation temperature that was also reported in other reports[26]. Figure 1c presents the UV–Vis absorption spectra of all prepared samples 10-folds diluted in toluene. In the case of precipitation temperature of 6 °C, only one excitonic absorption peak at 423 nm was observed and remained unchanged even after the temperature was further increased to 15 °C. As increasing the temperature up to 40 °C, broader absorption spectra with a band edge in the range of 480–520 nm were observed. A redshifted near band of its absorption spectra as increasing the precipitation temperature indicating the larger size of the perovskite[27]. The full width at half-maximum (FWHM) of its absorption band is around 12 nm, and the PL band is 25 nm, indicating a narrow distribution size. It suggested that the broader absorption spectra corresponded to the PQDs as reported in other reports[26,28,29], while the single sharp excitonic peaks at 423 nm are attributed to the PMSCs as well observed in other reports literatures[9,10,30].
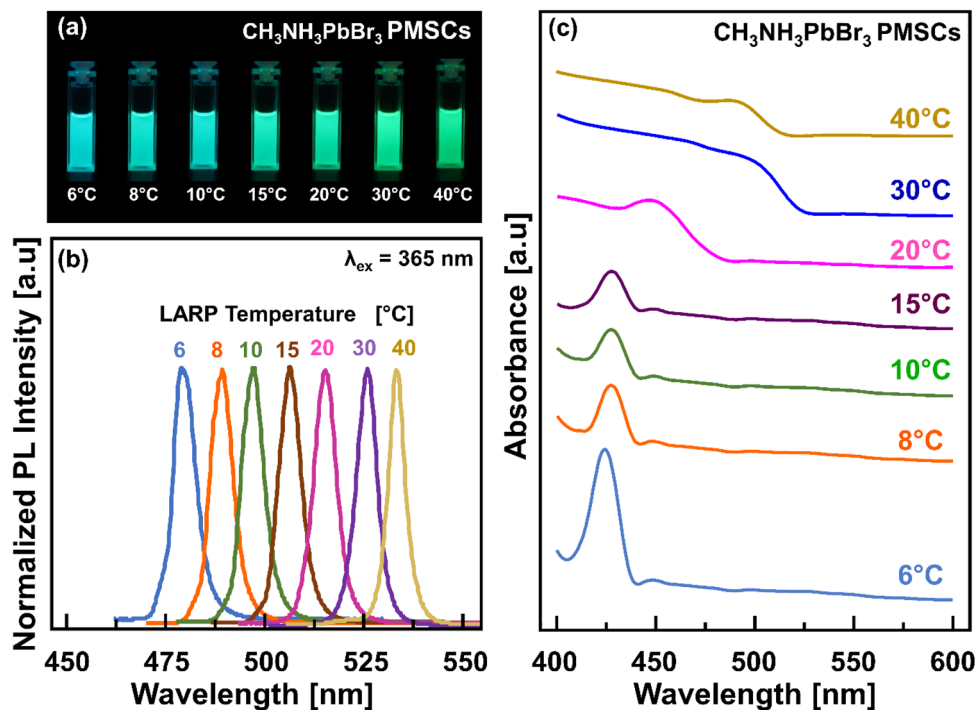
Figure 1. Optical properties of the as-synthesized $CH_3NH_3PbBr_3$ PMSCs in varying precipitation temperature. (**a**) Digital photograph of the luminescence of samples under 365 nm UV irradiation. (**b**) PL spectra of all samples under 365 nm UV excitation. (**c**). Optical absorption spectra of the samples.
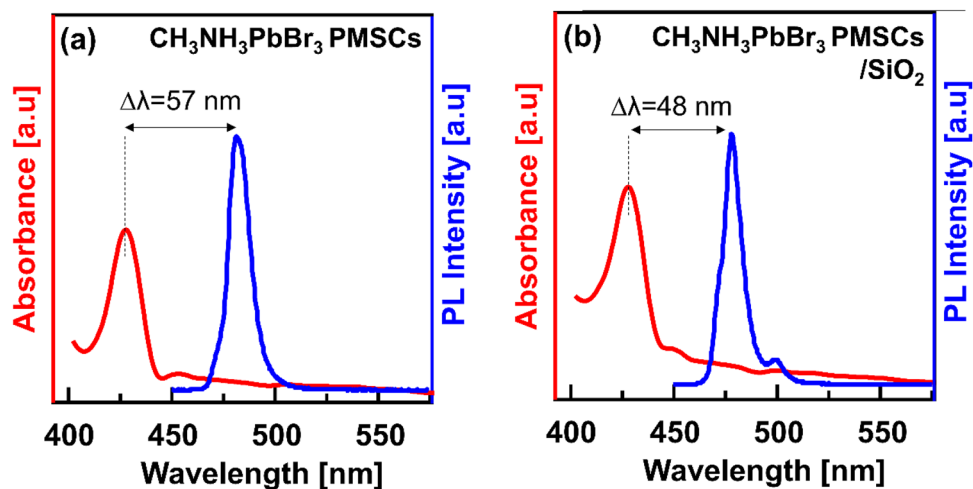

Figure 2. UV–Vis absorption and PL emission of the as-synthesized samples that synthesized at 6 °C. (**a**) $CH_3NH_3PbBr_3$ PMSCs. (**b**) $CH_3NH_3PbBr_3$ PMSCs/SiO_2.

Figure 2a presents the UV–Vis absorption and PL spectrum of the $CH_3NH_3PbBr_3$ PMSCs that synthesized at 6 °C. A relatively narrow emission spectrum (FWHM ~ 25 nm) indicating a very high colour purity that a preferable property for the display application[21]. A Stokes shifted of 57 nm might be attributed to the direct recombination process[26]. Despite a bright and tunable emission, the as-synthesized PMSCs are in a metastable state owing to their molecular-like behaviour. Then, a SiO_2 was used as a binder during the precipitation process of the PMSCs. The UV–Vis absorption and PL spectra of the $CH_3NH_3PbBr_3$ PMSCs/SiO_2 are shown in Fig. 2b. Intriguingly, a reduced Stokes shift (from 57 to 48 nm) of the PL emission relative to the excitonic absorption peak was observed. On the molecular-like particle, the stokes shift is linearly dependent on the Huang-Rhys factor (S), corresponding to the correlation between electron-vibrational coupling and chain length[31]. Empirically, $S = a\ exp\ (-n^2/b)$ where a and b are arbitrary constants and n is the number of atoms in the molecular system[31,32]. Then, the reduced stokes shifted of the $CH_3NH_3PbBr_3$ PMSCs/SiO_2 could possibly indicate the more rigid
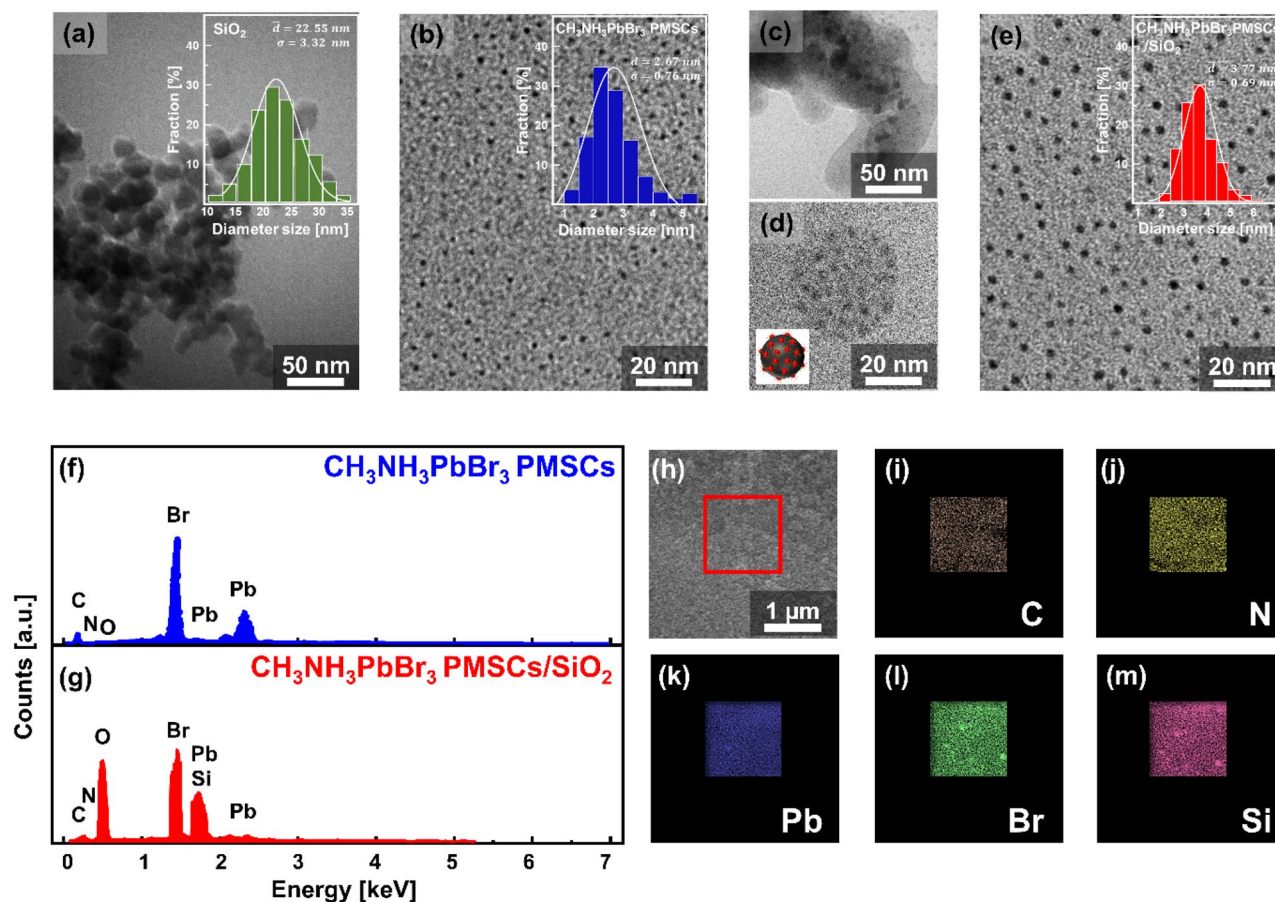
Figure 3. TEM images and its corresponded size distribution of the (**a**) SiO$_2$, (**b**) CH$_3$NH$_3$PbBr$_3$ PMSCs, (**c–e**) CH$_3$NH$_3$PbBr$_3$ PMSCs/SiO$_2$. EDS spectra of the (**f**) CH$_3$NH$_3$PbBr$_3$ PMSCs, (**g**) the CH$_3$NH$_3$PbBr$_3$ PMSCs/SiO$_2$. (**h–m**) EDS mapping analysis of the CH$_3$NH$_3$PbBr$_3$ PMSCs/SiO$_2$ showing the elemental distribution of carbon, nitrogen, lead, bromine, and silicon, respectively.

molecular structure induced by a larger molecular system or increased chain length on the surface of PMSCs[33,34]. It was reasonable with the presence of the SiO$_2$ during the precipitation process of the CH$_3$NH$_3$PbBr$_3$ PMSCs which indicate the incorporation of the SiO$_2$ to the PMSCs structure. The details of the incorporation of SiO$_2$ to the PMSCs structure will be further discussed. Intriguingly, a new shoulder PL emission appeared at 500 nm, attributing to the trap state of the CH$_3$NH$_3$PbBr$_3$ PMSCs composite or the smaller size PQDs formed[10]. However, a shoulder PL spectrum has not been observed for the CH$_3$NH$_3$PbBr$_3$ PMSCs without SiO$_2$ even after several days (Fig. S4). These results clearly point to the contribution of the SiO$_2$ nanoparticles to the shoulder emission peak of the CH$_3$NH$_3$PbBr$_3$ PMSCs.

Morphology and energy level of CH$_3$NH$_3$PbBr$_3$ PMSCs and CH$_3$NH$_3$PbBr$_3$ PMSCs/SiO$_2$. TEM measurement of the representative samples was conducted to evaluate the structural and morphological samples. The SiO$_2$ that used (Fig. 3a) shows spherical in agglomerated condition in diameter size of 22.55 ± 3.32 nm. In contrast, the CH$_3$NH$_3$PbBr$_3$ PMSCs sample (Fig. 3b) shows spherical dots in a uniform distribution in size of from 2.67 ± 0.67 nm. In the presence of the SiO$_2$ during the precipitation process, the CH$_3$NH$_3$PbBr$_3$ PMSCs was well composed with the SiO$_2$ (Fig. 3c). Interestingly, the PMSCs were well-distributed over the SiO$_2$ surfaces indicating the good synergetic effect of ligands with the SiO$_2$ surfaces (Fig. 3d). Furthermore, in the presence of the SiO$_2$, the PMSCs morphology are remained unchanged in spherical shapes with average diameter size of 3.77 ± 0.69 nm (Fig. 3e). The estimated diameter of the CH$_3$NH$_3$PbBr$_3$ PMSCs was calculated based on the Brus equation on the order of 2–4 nm[9]. While the CH$_3$NH$_3$PbBr$_3$ PMSCs size reported on the other previous reports commonly shows a slightly larger diameter size (5.0 ± 0.9 nm) than the estimated value that was calculated from Bruss model (around 2–4 nm) due to the aggregation induced by the electron microscopy preparations that could not be avoided[10]. Despite the shortcomings of the TEM measurement tools with regards to providing the precise structural and information of the Semiconductor Magic-sized Clusters[8,35–37] and the possibility aggregation of the sample during microscopy measurement, these as-synthesized PMSCs are in PMSCs range size with slightly smaller than other reports. Furthermore, the chemical composition of the PMSCs samples were characterized by Energy Dispersive X-ray Spectroscopy (EDS). Figure 3f showed the well-known elements of the C, O, Cs, Pb, and Br were identified in the CH$_3$NH$_3$PbBr$_3$ PMSCs sample, implying the CH$_3$NH$_3$PbBr$_3$ perovskite
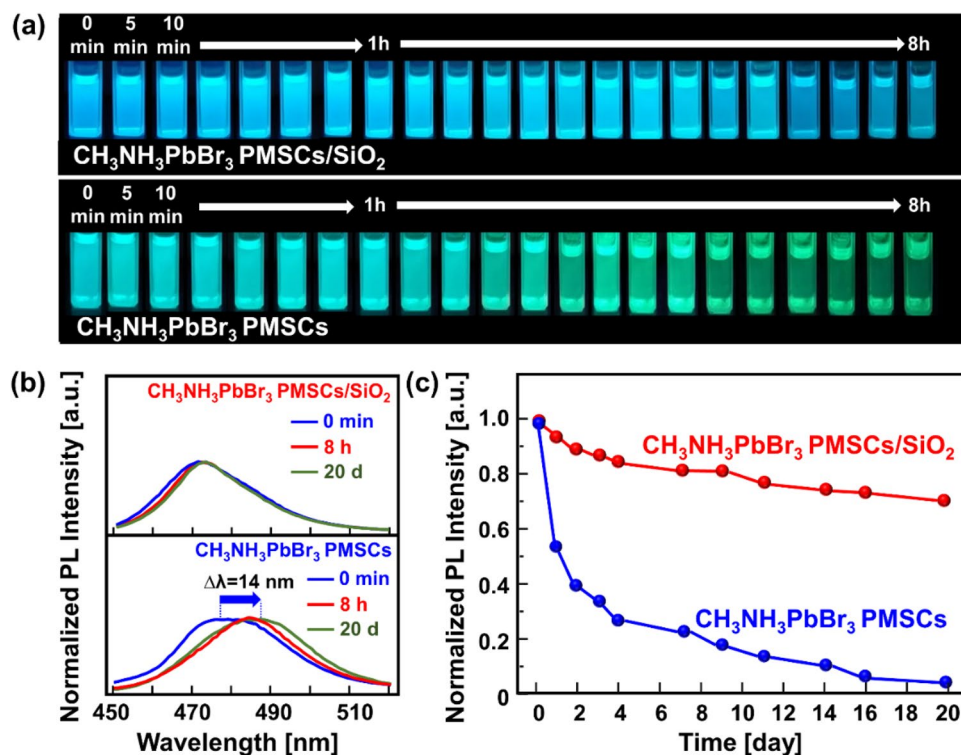
Figure 4. (**a**) Digital photograph of the CH$_3$NH$_3$PbBr$_3$ PMSCs and the CH$_3$NH$_3$PbBr$_3$ PMSCs/SiO$_2$ under elapsed-time observation in ambient condition for 8 h. (**b**) The emission PL spectra of the representative samples. (**c**) PL intensity of the samples that observed in ambient condition for 20 days.

structure. While the Si element peak emerges for the CH$_3$NH$_3$PbBr$_3$ PMSCs/SiO$_2$ sample (Fig. 3g), suggesting incorporating of the SiO$_2$ on the PMSCs sample. The corresponding elemental mapping of the selected area of CH$_3$NH$_3$PbBr$_3$ PMSCs/SiO$_2$ sample that marked in Fig. 3h, vividly shows the spatial distribution of the C, O, Cs, Pb, Br, and Si elements which are shown in (Fig. 3i–m).

The Effective Mass Approximation models proposed by Brus, was considered being applicable to PMSCs to estimate the bandgap energy of the PMSCs[9,38] as follows

$$E_{g(PMSCs)} = E_{g(bulk)} + \frac{h^2}{8r^2}\left(\frac{1}{m_e} + \frac{1}{m_h}\right) \tag{1}$$

where $E_{g(PMSCs)}$ is the bandgap energy of the PMSCs, $E_{g(bulk)}$ is the bandgap energy of the bulk material, h is the Planck's constant, r is the radius of the PMSCs, m_e is the effective mass of the electron and m_h is the effective mass of the hole. The bandgap energy of bulk properties was approximated by the Bulk CH$_3$NH$_3$PbBr$_3$ ($E_{g(bulk)} = 2.30$ eV),[39,40] and the effective mass of hole and electron was approximated by CH$_3$NH$_3$PbBr$_3$ based PMSCs from a previous report ($\left(\frac{1}{m_e} + \frac{1}{m_h}\right) = 2.37 \times 10^{30}$ kg^{-1})[9]. Using this relation and the size of the samples from TEM measurement, the bandgap energy of the CH$_3$NH$_3$PbBr$_3$ PMSCs and CH$_3$NH$_3$PbBr$_3$ PMSCs/SiO$_2$ are 2.49 and 2.39 eV, respectively. The precipitation process of PMSCs in the presence of SiO$_2$ generate the CH$_3$NH$_3$PbBr$_3$ PMSCs/SiO$_2$ with the bandgap energy slightly smaller than the only CH$_3$NH$_3$PbBr$_3$ PMSCs, owing to their quantum confinement effect. It was highly plausible because the hydroxyl groups on the SiO$_2$ could attract the amine-based ligand on the precursors that have not been formed into PMSCs structure, surpassing the nucleation and growth process. Thus, the perovskite nanostructure's particle size with the SiO$_2$ passivation is always bigger than the perovskite nanostructure itself that was also well-documented in other reports[19,41,42].

PL stability of CH$_3$NH$_3$PbBr$_3$ PMSCs and CH$_3$NH$_3$PbBr$_3$ PMSCs/SiO$_2$. The environmental stability of the PMSCs is a major research interest. To evaluate their stability, the relative PL intensities of the CH$_3$NH$_3$PbBr$_3$ PMSCs and CH$_3$NH$_3$PbBr$_3$ PMSCs/SiO$_2$ solutions were studied for 20 days in ambient conditions, with the results shown in Fig. 4. As shown in Fig. 4a, the PL emission of the CH$_3$NH$_3$PbBr$_3$ PMSCs/SiO$_2$ sample remains unchanged in blue emission for the first 8 h after synthesis process. While for the CH$_3$NH$_3$PbBr$_3$ PMSCs sample, the PL emission is redshifted on the blue-green region. This PL quenching is probably attributed to the ligand detachments owing to protonation and deprotonation reaction, inducing aggregation of PMSCs[43,44]. Another possibility is that the growth process of the PMSCs is still ongoing because the spherical PMSCs have relatively higher surface energy and thus grow at a slower rate[45,46].
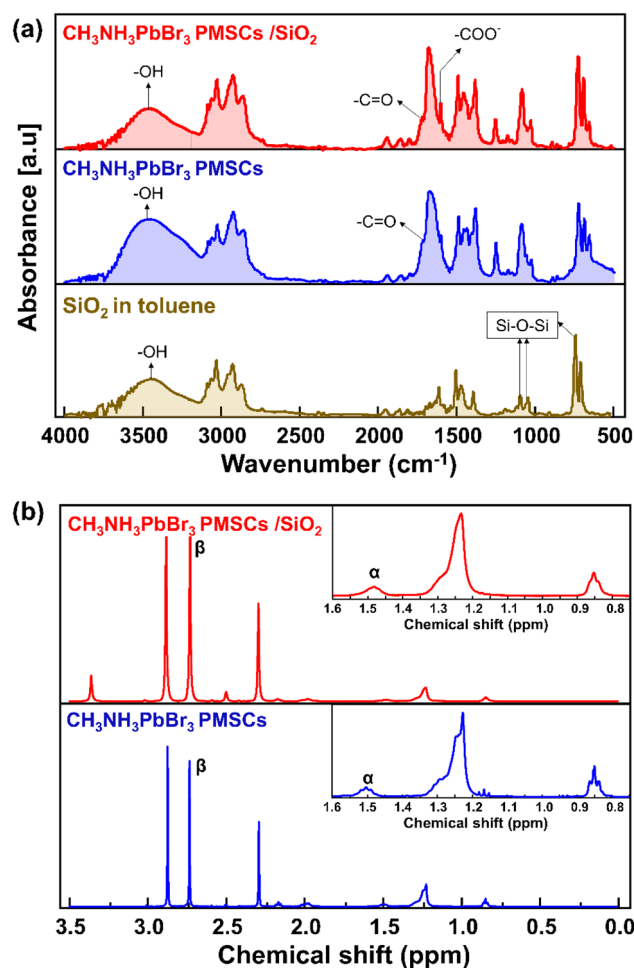
Figure 5. (**a**) FTIR Spectra of the SiO$_2$ in toluene, CH$_3$NH$_3$PbBr$_3$ PMSCs and CH$_3$NH$_3$PbBr$_3$ PMSCs/SiO$_2$. (**b**) ^{1}H spectra of the CH$_3$NH$_3$PbBr$_3$ PMSCs and CH$_3$NH$_3$PbBr$_3$ PMSCs/SiO$_2$ in deuterated DMSO. The inset figure is the magnification of the ^{1}H spectra on the chemical shift range 0.8–1.6 ppm showing the broadening peaks for the CH$_3$NH$_3$PbBr$_3$ PMSCs/SiO$_2$.

Figure 4b shows the corresponding emission spectra of samples for 20 days of observation. The CH$_3$NH$_3$PbBr$_3$ PMSCs/SiO$_2$ sample emission peak remains constant, while the emission peak of the CH$_3$NH$_3$PbBr$_3$ PMSCs was continuously redshifted as much of 14 nm. Figure 4c shows the PL intensity quenching with time for samples. The PL quenching of the CH$_3$NH$_3$PbBr$_3$ PMSCs in air induced by chemical instability on the PMSCs surface[47].

Even though the Oleic Acid and Oleylamine was used as ligand, the combination of both ligands promptly undergoes aggregation, sedimentation and degradation. This phenomenon is attributed to the high probability of proton transfer from oleic acid to Oleylamine, inducing the detachment of Oleylamine from the surface of the PMSCs[43,44]. Thus, the as-synthesized CH$_3$NH$_3$PbBr$_3$ PMSCs suffered poor stability *i.e.*, degraded completely in 20 days indicated by the vanished luminescence in ambient condition. In contrast, the CH$_3$NH$_3$PbBr$_3$ PMSCs/SiO$_2$ exhibit a slow quenching in PL intensity and retained a high value (70% of the initial intensity) after 20 days. It is pointed out that the SiO$_2$ enhanced the stability of the CH$_3$NH$_3$PbBr$_3$ PMSCs, which should be due to the passivation of PMSCs surfaces.

The interaction mechanism of the PMSCs surface with the SiO$_2$ was studied by Fourier Transform Infrared (FTIR). The FTIR spectra of the SiO$_2$ dispersed in toluene, CH$_3$NH$_3$PbBr$_3$ PMSCs and the CH$_3$NH$_3$PbBr$_3$ PMSCs/SiO$_2$ are shown in Fig. 5a. The FTIR spectrum of SiO$_2$ in toluene demonstrates the strong peaks absorption at 800, 1087 and 1087 cm^{-1} that attributed to the Si–O–Si bonds. Also, the peak at 3430 cm^{-1} indicates the presence of Si–OH bonds on the SiO$_2$ surfaces which is typically resulted interaction between toluene and the SiO$_2$ surfaces[48,49]. In the CH$_3$NH$_3$PbBr$_3$ PMSCs spectrum, the peak at 1729 cm^{-1} corresponds to C=O that a typically present in the Oleic Acid-modified Nanoparticle. The N–H stretching and C–C bond can be seen at around 3321 and 1652 cm^{-1}, although the band overlaps with the –OH band, typically present in the Oleylamine-modified Nanoparticle[50]. It indicates that the as-synthesized CH$_3$NH$_3$PbBr$_3$ PMSCs was well-capped by the Oleic acid and Oleylamine ligand. In addition of SiO$_2$, the –COOH vibration peak at 1729 cm^{-1} and –OH vibration peak at 3430 cm^{-1} decreases, while a peak at 1590 cm^{-1} corresponding to COO$^-$ (carboxylate) ions increase significantly. Thus, it could be suggested that the –C=O on the surface of CH$_3$NH$_3$PbBr$_3$ PMSCs has reacted with the –OH on the surface of SiO$_2$, resulted more carboxylate ions.
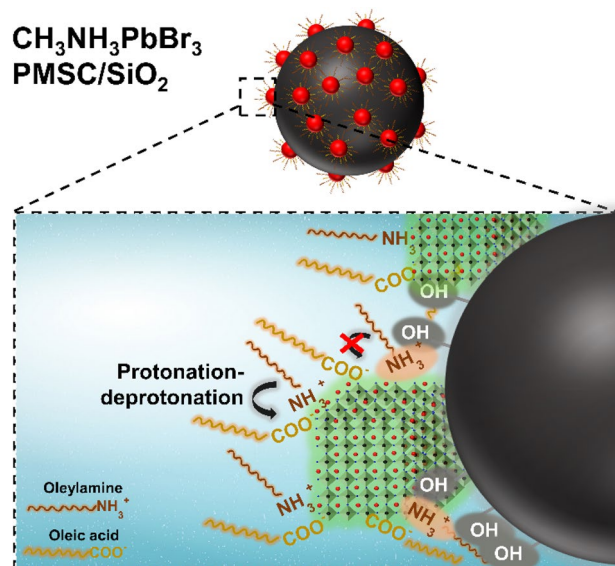
Figure 6. Illustration of the surface passivation of the $CH_3NH_3PbBr_3$ PMSCs by SiO_2 and oleylamine and oleic acid ligands.

To investigate the interaction between the ligand species and the hydroxyl groups on the surface of SiO_2, the ^1H NMR solution was conducted. Comparing with the ^1H spectra of the used ligand species (Fig. S5), Fig. 5b shows the characteristics resonances of the Oleic acid and Oleylamine in all samples, suggesting a well-capping of the PMSCs by these ligands consistent with the FTIR spectra in Fig. 5a. It is worth to noting that the α resonances has been shifted from 1.474 ppm from the $CH_3NH_3PbBr_3$ PMSCs to 1.490 ppm for $CH_3NH_3PbBr_3$ PMSCs/SiO_2, indicating the amine-groups on the perovskite surface interact with the silica surfaces[51]. Furthermore, we have evaluated the ^1H spin–spin (T_2) relaxation measurement that is sensitive to the dynamically dipole–dipole interaction between molecules in solvent[46,52,53]. The T_2 relaxation time attributes to the required time of the molecules in the solution to return to an initial equilibrium state after a dynamic motion by an electromagnetic radiation[52]. The spin–spin (T_2) relaxation measurement (Table S1) shows that all ^1H NMR signal in the range of 0–3.5 ppm of the $CH_3NH_3PbBr_3$ PMSCs/SiO_2 has faster relaxation times than those $CH_3NH_3PbBr_3$ PMSCs. The detailed implication of the T_2 relaxation time will be discussed further in discussion section.

Discussion

PMSCs structure typically suffers a metastable phase since their poor passivation due to their smaller size and large surface/volume ratio. In a common pathway, the PMSCs formation during precipitation is reversible with the PQDs formation[8,30]. While the PQDs easily undergo aggregation, sedimentation, and degradation in ambient condition. A poor stability of PMSCs corresponds to its surface defect on Pb^{2+}, Br^-, and $CH_3NH_3^+$ sites. In $CH_3NH_3PbBr_3$ PMSCs sample, a high concentration of the oleic acid and oleylamine are used in conjunction ligands. The amine-based ligand was usually used to passivate the Pb^{2+} and $CH_3NH_3^+$ defects by exploits a lone pair electron of the N atoms. An excessive amine-based ligand could generate more ammonium cation $\left(NH_3^+\right)$, to passivate the Br^- defects on the surfaces. In addition, amine-based ligand can deprotonate carboxylic acid (from Oleic Acid) into carboxylate ion, COO^- that should effectively passivate Pb^{2+} and $CH_3NH_3^+$ defects. The protonation-deprotonation reaction between Oleic acid and Oleylamine ligand that might be possibly occurred can be described by Eq. (2)

$$R - COOH + R' - NH_2 \leftrightarrow R - COO^- + R' - NH_3^+ \tag{2}$$
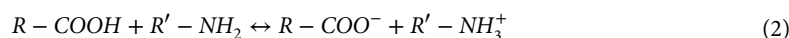
However, a reversible protonation-deprotonation reaction could increase the possibility of the ligand detachment from the PMSCs surface, leading a poor stability. Addition of the SiO_2 enriched with OH groups on the surfaces to the system, induced the chemical reaction with the $R - COOH$ and R-NH_2 via dipole–dipole interaction as observed by the chemical shift of the ^1H spectra of the α and β resonance to the higher values that was indicated by the chemical shift toward higher value (Fig. 5b)[51,54]. This interaction shifted the equilibrium protonation-deprotonation reaction into other side, generating more carboxylate ions, COO^- [49]. An abundant carboxylate ion which was detected by the increased absorbance IR spectrum at 1590 cm^{-1} as shown in Fig. 5a, is expected to effectively passivate PMSCs surface defect. The spherical PMSCs has relatively higher surface energy and thus grows at a slower rate[45]. Then, the addition of the SiO_2 that has a high specific surface area, inducing the growth PMSCs that is still undergoing are prone to attach to the surface of SiO_2[18]. The PMSCs attached on the SiO_2 surface via both ion–dipole and dipole–dipole interaction, was also observed as the faster (lower T_2 value) of the overall T_2 relaxation times of the $CH_3NH_3PbBr_3$ PMSC/SiO_2 in the range of 0–3.5 ppm (Table S1). The faster of the T_2 relaxation times, the more PMSC are non-covalently bound on the SiO_2 surface[53]. Thus, the

PMSCs attachment on the surfaces helps ensure the crystal structure in humid condition and prevent the PL quenching of these PMSCs. The surface passivation of the PMSCs by SiO_2 and an excessed surface ligand was illustrated in Fig. 6.

Conclusions

In summary, $CH_3NH_3PbBr_3$ PMSCs was synthesized by utilising of an excess concentration of capping ligands i.e., oleylamine and oleic acid and SiO_2 addition through a ligand assisted re-precipitation method. The synergetic effect of the ligand and SiO_2 was investigated systematically. For the PMSCs samples without SiO_2 addition, the PL emission was vanished, while with the SiO_2 addition, the PL emission retained 70% of its initial emission intensity in ambient condition for 20 days. FTIR analysis was conducted to investigate the surface ligand composition and the underlying mechanism. We suggest that the SiO_2 enriched with OH groups on the PMSCs surfaces induced the chemical reaction with the $R-COOH$ generating more carboxylate ion, COO^-. These abundant carboxylate ions could effectively passivate the PMSCs surface by inhibiting the protonation-deprotonation between the amine and acid-based ligands, lead an enhanced PL stability than the PMSCs without SiO_2. This study provides a deeper insight into the metastability phenomenon of the PMSCs at ambient condition. It has important implications in understanding and controlling nucleation and growth of semiconductor nanoparticles through a reliable characterization of PMSCs.

Methods

Materials. Lead(II) Bromide ($PbBr_2$, ≥ 98%, Sigma Aldrich, Singapore Ltd.), Methylamine Bromide ($CH_3NH_3PbBr_3$, 98%, Sigma Aldrich, Singapore Ltd.), Oleylamine ($C_{18}H_{35}NH_2$, 70%, Sigma Aldrich, Singapore), Oleic acid ($C_{18}H_3O_2$, Sigma Aldrich, Singapore), Anhydrous N,N-Dymethylformamide ($C_3H_8N_2$, Merck Ltd., Indonesia), Toluene (C_7H_8, Merck Ltd., Indonesia Ltd.), Fumed Silica (SiO_2, 98%, Aerosil 380, Evonik Ltd., Singapore). All materials were used without further purification.

Synthesis of $CH_3NH_3PbBr_3$ PMSCs. $CH_3NH_3PbBr_3$ PMSCs was synthesized by a ligand assisted co-precipitation that was reported elsewhere[26]. In brief, a mixture containing of 0.4 mmol of PbBr2 that was dissolved in dimethylformamide (DMF), 0.4 mmol oleylamine, 3 mmol oleic acid, and 0.32 mmol $CH_3NH_3Br_2$ in DMF was sonicated by an ultra-sonication. Then, 10% (v/v) of the precursor was precipitated in toluene that was precooled or preheated under vigorous stirring. Precipitation temperature was varying to obtain the tunable emission of PMSCs. The obtained solution turned into thick yellow color and exhibited a luminescence. Centrifugation was conducted to remove the by-product from the obtained the colloidal $CH_3NH_3PbBr_3$ PMSCs. A syringe filtration 0.22 μm (RC membrane, Satorius Co.) was performed as the last step of sample purification for further characterizations.

Synthesis of $CH_3NH_3PbBr_3$ PMSCs /SiO_2. A fumed silica, SiO_2 (10 wt.%) was dispersed in toluene under vigorous stirring at room temperature. Subsequently, 20% (v/v) of SiO_2 mixture was added into the precipitated PMSCs immediately, resulted $CH_3NH_3PbBr_3$ PMSCs/SiO_2. Centrifugation was conducted to remove the by-product from the obtained the colloidal $CH_3NH_3PbBr_3$ PMSCs/SiO_2. A syringe filtration 0.22 μm (RC membrane, Satorius Co.) was performed as the last step of sample purification for further characterizations.

Characterization. Ultraviolet–visible (UV–Vis) absorbance spectra were measured by an Ocean Optic, D-2000 using a quartz cuvette with 10 mm optical path length at room temperature. The PL spectra of the samples were measured by an Agilent Cary eclipse spectrofluorometer with a Xenon lamp as light source. Transmission Electron Microscopy (TEM) characterization was conducted by drop-casting samples solution on a commercial EM Grid with Copper coating operated at acceleration voltage 120 kV using Hitachi HT7700. Energy-dispersive X-ray spectroscopy (EDS) was conducted by JEOL JSM 6510 operated at acceleration voltage 15 kV. The sample solution was dropped onto a KBr pellet to conduct the Fourier Transform Infra-Red (FTIR) measurement using IR Prestige-21 FTIR Spectrometer (Shimadzu, a spectra resolution of 1 cm^{-1}). ^{1}H NMR spectra was recorded by 500 MHz NMR Agilent DD2 Spectrometer (Agilent Technologies) in deuterated DMSO.

References

1. Harrell, S. M., McBride, J. R. & Rosenthal, S. J. Synthesis of ultrasmall and magic-sized CdSe nanocrystals. *Chem. Mater.* **25**, 1199–1210 (2013).
2. Evans, C. M., Guo, L., Peterson, J. J., Maccagnano-Zacher, S. & Krauss, T. D. Ultrabright PbSe magic-sized clusters. *Nano Lett.* **8**, 2896–2899 (2008).
3. Ning, J. & Banin, U. Magic size InP and InAs clusters: Synthesis, characterization and shell growth. *Chem. Commun.* **53**, 2626–2629 (2017).
4. Zhang, B. *et al.* Thermally-induced reversible structural isomerization in colloidal semiconductor CdS magic-size clusters. *Nat. Commun.* **9**, 1–10 (2018).
5. Park, Y. J. *et al.* Light-emitting transistors with high color purity using perovskite quantum dot emitters. *ACS Appl. Mater. Interfaces* **12**, 35175–35180 (2020).
6. Jancik Prochazkova, A. *et al.* Proteinogenic amino acid assisted preparation of highly luminescent hybrid perovskite nanoparticles. *ACS Appl. Nano Mater.* **2**, 4267–4274 (2019).

7. Kim, J. Y., Lee, J. W., Jung, H. S., Shin, H. & Park, N. G. High-efficiency perovskite solar cells. *Chem. Rev.* **120**, 7867–7918 (2020).
8. Palencia, C., Yu, K. & Boldt, K. The future of colloidal semiconductor magic-size clusters. *ACS Nano* **14**, 1227–1235 (2020).
9. Vickers, E. T. *et al.* Ligand dependent growth and optical properties of hybrid organo-metal halide perovskite magic sized clusters. *J. Phys. Chem. C* **123**, 18746–18752 (2019).
10. Liu, L. *et al.* Varying the concentration of organic acid and amine ligands allows tuning between quantum dots and magic-sized clusters of $CH_3NH_3PbBr_3$ perovskite: Implications for photonics and energy conversion. *ACS Appl. Nano Mater.* **3**, 12379–12387 (2020).
11. Singh, A. N. *et al.* Interface engineering driven stabilization of halide perovskites against moisture, heat, and light for optoelectronic applications. *Adv. Energy Mater.* **10**, 2000768 (2020).
12. Xu, K. *et al.* First synthesis of Mn-doped cesium lead bromide perovskite magic sized clusters at room temperature. *J. Phys. Chem. Lett.* **11**, 1162–1169 (2020).
13. Ham, D. S. *et al.* Influence of drying conditions on device performances of antisolvent-assisted roll-to-roll slot die-coated perovskite solar cells. *ACS Appl. Energy Mater.* **4**, 7611–7621 (2021).
14. Yang, D. *et al.* CsPbBr 3 quantum dots 20: Benzenesulfonic acid equivalent ligand awakens complete purification. *Adv. Mater.* **31**, 1900767 (2019).
15. Wu, Y., Yan, M., Cui, J., Yan, Y. & Li, C. A multiple-functional Ag/SiO_2/organic based biomimetic nanocomposite membrane for high-stability protein recognition and cell adhesion/detachment. *Adv. Funct. Mater.* **25**, 5823–5832 (2015).
16. Qiu, L. *et al.* Highly efficient and stable $CsPbBr_3$ perovskite quantum dots by encapsulation in dual-shell hollow silica spheres for WLEDs. *Inorg. Chem. Front.* **7**, 2060–2071 (2020).
17. Wang, J., Li, M., Shen, W., Su, W. & He, R. Ultrastable carbon quantum dots-doped $MAPbBr_3$ perovskite with silica encapsulation. *ACS Appl. Mater. Interfaces* **11**, 34348–34354 (2019).
18. Zhang, F. *et al.* Synergetic effect of the surfactant and silica coating on the enhanced emission and stability of perovskite quantum dots for anticounterfeiting. *ACS Appl. Mater. Interfaces* **11**, 28013–28022 (2019).
19. Yang, M. *et al.* In situ silica coating-directed synthesis of orthorhombic methylammonium lead bromide perovskite quantum dots with high stability. *J. Colloid Interface Sci.* **509**, 32–38 (2018).
20. Huang, S. *et al.* Enhancing the stability of CH3NH3PbBr3 quantum dots by embedding in silica spheres derived from tetramethyl orthosilicate in 'waterless' toluene. *J. Am. Chem. Soc.* **138**, 5749–5752 (2016).
21. Dirin, D. N. *et al.* Harnessing defect-tolerance at the nanoscale: Highly luminescent lead halide perovskite nanocrystals in mesoporous silica matrixes. *Nano Lett.* **16**, 5866–5874 (2016).
22. Li, S. *et al.* Water-resistant perovskite nanodots enable robust two-photon lasing in aqueous environment. *Nat. Commun.* **11**, 1–8 (2020).
23. Malgras, V. *et al.* Observation of quantum confinement in monodisperse methylammonium lead halide perovskite nanocrystals embedded in mesoporous silica. *J. Am. Chem. Soc.* **138**, 13874–13881 (2016).
24. Chen, P. *et al.* In situ growth of ultrasmall cesium lead bromine quantum dots in a mesoporous silica matrix and their application in flexible light-emitting diodes. *Nanoscale* **11**, 16499–16507 (2019).
25. Nakamura, Y., Fujinoki, N. & Ichikawa, M. Photoluminescence from Si-capped GeSn nanodots on Si substrates formed using an ultrathin SiO 2 film technique. *J. Appl. Phys.* **106**, 14309 (2009).
26. Huang, H., Susha, A. S., Kershaw, S. V., Hung, T. F. & Rogach, A. L. Control of emission color of high quantum yield CH3NH3PbBr3 perovskite quantum dots by precipitation temperature. *Adv. Sci.* **2**, (2015).
27. Kim, T., Jung, S.I., Ham, S., Chung, H. & Kim, D. Elucidation of photoluminescence blinking mechanism and multiexciton dynamics in hybrid organic-inorganic perovskite quantum dots. *Small* **15**, 1900355 (2019).
28. Vickers, E. T. *et al.* Enhancing charge carrier delocalization in perovskite quantum dot solids with energetically aligned conjugated capping ligands. *ACS Energy Lett.* **5**, 817–825 (2020).
29. Huang, H. *et al.* Growth mechanism of strongly emitting CH3NH3PbBr 3 perovskite nanocrystals with a tunable bandgap. *Nat. Commun.* **8**, 1–8 (2017).
30. Zhang, J. *et al.* Individual pathways in the formation of magic-size clusters and conventional quantum dots. *J. Phys. Chem. Lett.* **9**, 3660–3666 (2018).
31. O'Neill, L. & Byrne, H. J. Structure-property relationships for electron-vibrational coupling in conjugated organic oligomeric systems. *J. Phys. Chem. B* **109**, 12685–12690 (2005).
32. De Jong, M., Seijo, L., Meijerink, A. & Rabouw, F. T. Resolving the ambiguity in the relation between Stokes shift and Huang-Rhys parameter. *Phys. Chem. Chem. Phys.* **17**, 16959–16969 (2015).
33. Lao, X. *et al.* Anomalous temperature-dependent exciton-phonon coupling in cesium lead bromide perovskite nanosheets. *J. Phys. Chem. C* **123**, 5128–5135 (2019).
34. Siddique, H. *et al.* Anomalous octahedron distortion of bi-alloyed Cs2AgInCl6Crystal via XRD, Raman, Huang-Rhys factor, and photoluminescence. *J. Phys. Chem. Lett.* **11**, 9572–9578 (2020).
35. Wan, W. *et al.* Room-temperature formation of CdS magic-size clusters in aqueous solutions assisted by primary amines. *Nat. Commun.* **11**, 1–8 (2020).
36. Wang, L. *et al.* Precursor self-assembly identified as a general pathway for colloidal semiconductor magic-size clusters. *Adv. Sci.* **5**, 1800632 (2018).
37. Gao, D. *et al.* Formation of colloidal alloy semiconductor CdTeSe magic-size clusters at room temperature. *Nat. Commun.* **10**, 1–9 (2019).
38. Chukwuocha, E. O., Onyeaju, M. C. & Harry, T. S. T. Theoretical studies on the effect of confinement on quantum dots using the brus equation. *World J. Condens. Matter Phys.* **02**, 96–100 (2012).
39. Naghadeh, S. B. *et al.* Size dependence of charge carrier dynamics in organometal halide perovskite nanocrystals: Deciphering radiative versus nonradiative components. *J. Phys. Chem. C* **123**, 4610–4619 (2019).
40. Sheng, R. *et al.* Methylammonium lead bromide perovskite-based solar cells by vapor-assisted deposition. *J. Phys. Chem. C* **119**, 3545–3549 (2015).
41. Zhang, C. *et al.* Exciton photoluminescence of CsPbBr 3 @SiO 2 quantum dots and its application as a phosphor material in light-emitting devices. *Opt. Mater. Express* **10**, 1007 (2020).
42. Zhang, F. *et al.* Silica coating enhances the stability of inorganic perovskite nanocrystals for efficient and stable down-conversion in white light-emitting devices. *Nanoscale* **10**, 20131–20139 (2018).
43. Akkerman, Q. A. *et al.* Solution synthesis approach to colloidal cesium lead halide perovskite nanoplatelets with monolayer-level thickness control. *J. Am. Chem. Soc.* **138**, 1010–1016 (2016).
44. Iso, Y. & Isobe, T. Review—Synthesis, luminescent properties, and stabilities of cesium lead halide perovskite nanocrystals. *ECS J. Solid State Sci. Technol.* **7**, R3040–R3045 (2018).
45. Moon, J. *et al.* Surface energy-driven preferential grain growth of metal halide perovskites: Effects of nanoimprint lithography beyond direct patterning. *ACS Appl. Mater. Interfaces* **13**, 5368–5378 (2021).
46. Brown, A. A. M. *et al.* Precise control of CsPbBr 3 perovskite nanocrystal growth at room temperature: Size tunability and synthetic insights. *Chem. Mater.* **33**, 2387–2397 (2021).
47. Kuhs, J. *et al.* In situ photoluminescence of colloidal quantum dots during gas exposure—The role of water and reactive atomic layer deposition precursors. *ACS Appl. Mater. Interfaces* **11**, 26277–26287 (2019).

48. Gun'Ko, V. M., Vedamuthu, M. S., Henderson, G. L. & Blitz, J. P. Mechanism and kinetics of hexamethyldisilazane reaction with a fumed silica surface. *J. Colloid Interface Sci.* **228**, 157–170 (2000).
49. Li, Z. & Zhu, Y. Surface-modification of SiO$_2$ nanoparticles with oleic acid. *Appl. Surf. Sci.* **211**, 315–320 (2003).
50. Guo, H. *et al.* Shape-selective formation of monodisperse copper nanospheres and nanocubes via disproportionation reaction route and their optical properties. *J. Phys. Chem. C* **118**, 9801–9808 (2014).
51. Chen, Y. *et al.* Overcoming the anisotropic growth limitations of free-standing single-crystal halide perovskite films. *Angew. Chemie Int. Ed.* **60**, 2629–2636 (2021).
52. Aiello, F. & Masi, S. The contribution of NMR spectroscopy in understanding perovskite stabilization phenomena. *Nanomater.* **11**, 2024 (2021).
53. Yuan, L., Chen, L., Chen, X., Liu, R. & Ge, G. In situ measurement of surface functional groups on silica nanoparticles using solvent relaxation nuclear magnetic resonance. *Langmuir* **33**, 8724–8729 (2017).
54. Hassanabadi, E. *et al.* Ligand & band gap engineering: tailoring the protocol synthesis for achieving high-quality CsPbI3 quantum dots. *Nanoscale* **12**, 14194–14203 (2020).

Acknowledgements

Author contributions

Competing interests

The authors declare no competing interests.

Additional information

Supplementary Information The online version contains supplementary material available at https://doi.org/10.1038/s41598-021-01560-4.

Correspondence and requests for materials should be addressed to F.I.

Reprints and permissions information is available at www.nature.com/reprints.

Publisher's note Springer Nature remains neutral with regard to jurisdictional claims in published maps and institutional affiliations.